Journal of the Australian Ceramic Society (2020) 56:631–638
https://doi.org/10.1007/s41779-019-00379-7

RESEARCH

Effect of metallic content on sintering behavior of $NiFe_2O_4$-based cermet inert anode for aluminum electrolysis

Zhigang Zhang[1] · Xiaotong Lu[1] · Jianrong Xu[1] · Zhuokun Cao[1] · Hongjie Luo[1]

Received: 13 November 2018 / Revised: 5 April 2019 / Accepted: 28 May 2019 / Published online: 8 June 2019

Abstract

In order to overcome the high carbon consumption and serious environmental pollution as a result of adopting consumable carbon anode, $NiFe_2O_4$-based cermet inert anode for aluminum electrolysis was prepared by powder metallurgy method using 85Cu-15Ni binary alloy as metallic phase. The metallic phase content was varied from 0 to 20 (mass fraction, %) with 5% intervals. The effect of metallic phase content on sintering behavior and microstructure was investigated by a thermal dilatometer and field emission scanning electron microscopy. The results show that the maximum linear shrinkage and linear shrinkage rates enhance with the increase of the metallic phase content, while the temperature of maximum linear shrinkage rate shows the opposite changing law. The sintering activation energy of the initial stage lowers from 471.13 to 236.47 $kJ \cdot mol^{-1}$ with the metallic additive range from 0 to 20%. The introduction of metallic phase could effectively enhance the grain boundary bonding strength and increase the grain size step by step.

Keywords Inert anode · $NiFe_2O_4$, · Cermet · Shrinkage, · Sintering activation energy

Introduction

It is well-known that the Hall-Héroult process, developed in 1886, is the only commercial method for production of aluminum from alumina. Though the techniques and equipments and many other aspects have greatly improved in the process of aluminum electrolysis, the use of carbon anode has not changed till now. Sufficient attention has been focused on the disadvantages caused by using carbon anode for aluminum electrolysis, such as carbon wasting and environmental pollution. Inert anode has been reckoned as the ideal anode for aluminum electrolysis for its significant environmental benefits, only producing environment-friendly O_2 gas instead of greenhouse gas (carbon dioxide) and fluorocarbons [1–4].

Up to now, despite intensive research efforts that have been made, no fully satisfactory inert anode material has been found to meet all commercial requirements. Compared with oxides ceramics and metals, $NiFe_2O_4$-based cermets are a promising candidate as an inert anode for aluminum electrolysis, due to their putative ability to combine the features of $NiFe_2O_4$ ceramics and metals, namely, high thermodynamic stability and high corrosion resistance against fluoride melts as well as high electronic conductivity [5–11].

$Cu/NiFe_2O_4$ cermets containing various mass fractions of Cu were prepared by conventional cold isostatic pressing-sintering process and their electrical conductivities obeyed the rule of semiconductor electrical mechanism [12]. Tian et al. [13, 14] studied the effect of Ni content on the corrosion resistance and electrical conductivity of $Ni/NiFe_2O_4$ cermet inert anodes, and the proper Ni content in ceramic phase was determined to be 5% (mass fraction). Ag was added to prepare $Ag/NiFe_2O_4$ cermet and the introduction of Ag can promote sintering and improve availably mechanical properties and electrical conductivity [15]. Copper-nickel binary alloy was supposed to an ideal metallic phase to improve the wettability between metal and ceramic, exhibiting better sintering performance. As a result, copper-nickel binary alloy became the most promising metallic phase for $NiFe_2O_4$-based cermet inert anode, and current researches on $NiFe_2O_4$-based cermet inert anode mainly focused on the mechanical and electrical properties as well as corrosion resistance [16, 17]. However, to the best of our knowledge, the effect of metallic phase content on sintering behavior of $NiFe_2O_4$-based cermet inert anode has few been discussed in detail so far.

✉ Zhigang Zhang
zhangzg@smm.neu.edu.cn

[1] School of Metallurgy, Northeastern University, Shenyang 110819, Liaoning, People's Republic of China

The properties of $NiFe_2O_4$-based cermet are controlled by microstructure, which is closely related to the sintering process. The composition of cermet plays a dominant role on sintering behavior. The variation of a metallic phase, which would become a liquid phase during sintering, can significantly affect the kinetics of densification and grain growth, grain boundary motion, pore mobility, and pore removal [18]. So it is necessary to conduct a systematic study on the effect of metallic phase content on sintering behavior of $NiFe_2O_4$-based cermet inert anode.

In this study, $NiFe_2O_4$-based cermet inert anodes, with copper-nickel binary alloy content of 0, 5%, 10%, 15%, and 20% (mass fraction), were fabricated by cold pressing and sintering. The purpose of this work is to investigate the effect of metallic phase content on sintering behavior and microstructure of $NiFe_2O_4$-based cermet inert anodes.

Materials and experimental techniques

Raw materials

Nickel monoxide (NiO ≥ 99.0%), iron sesquioxide (Fe_2O_3 ≥ 99.0%), nickel powder (Ni ≥ 99.5%), copper powder (Cu ≥ 99.7%), manganese dioxide (MnO_2 ≥ 97.5%), vanadium pentoxide (V_2O_5 ≥ 99.0%), polyvinyl alcohol (PVA ≥ 99.0%), and absolute ethyl alcohol (CH_3CH_2OH ≥ 99.5%) were purchased from Sinopharm Chemical Reagent Co., Ltd. (Shanghai, China). All the adoptive chemicals in this study were of analytical grade and used as received without further purification. Distilled water was used as a solvent.

Specimen preparation

Two-step sintering was adopted to prepare $NiFe_2O_4$-based cermet inert anode. Firstly, a proper amount of Fe_2O_3 and NiO powders (the excess content of NiO in the ceramic phase, compared with that of the stoichiometric $NiFe_2O_4$, is 15%, mass fraction), with 1% MnO_2 and 0.5% V_2O_5, was mixed in planetary muller for 24 h using distilled water as dispersant. The dried mixtures with 4% PVA binder were molded by cold pressing under 60 MPa into Φ100 mm circular cylinder and then calcined in a muffle furnace at 1000 °C for 6 h in air to form the 15NiO-85$NiFe_2O_4$ matrix block materials. After crushing and screening, 15NiO-85$NiFe_2O_4$ powders with particle size below 74 μm were obtained. Secondly, the obtained 15NiO-85$NiFe_2O_4$ ceramic powders were then mixed with different contents (0, 5%, 10%, 15%, 20%) of 85Cu-15Ni powders by ball milling using absolute ethyl alcohol as dispersant to avoid metal oxidation. After drying in a vacuum-drying oven and grinding with a 4% PVA binder, the well-mixed ceramic-metal powders were cold pressed under 200 MPa into two types of blocks, namely *Φ*10-mm-circular cylinder and 60 mm × 15 mm × 8-mm-rectangular solid.

Sintering experiment

Sintering linear shrinkage behaviors of the green bodies (*Φ*10-mm-circular cylinder) with different metallic phase amounts were respectively measured by the horizontal dilatometer (Netzsch, DIL402 PC, Germany) in a nitrogen shield atmosphere. During the sintering experiment, all samples were heated at different constant rates (namely 5, 10, and 20 °C/min) to 1300 °C and then furnace cooled down to ambient temperature.

Green bodies (60 mm × 15 mm × 8-mm-rectangular solid) were respectively sintered to desired temperatures by self-made high temperature vacuum-sintering furnace in a nitrogen shield atmosphere and then furnace cooled down to ambient temperature.

Characterization

Phase transition in NiO-$NiFe_2O_4$-Cu-Ni system was analyzed in a TGA/DSC simultaneous thermal analyzer (Netzsch, STA 449 F3 Jupiter, Germany). The experiment was performed from ambient temperature up to the maximum temperature of 1300 °C at the constant heating rate of 10 °C/min in the atmosphere of argon.

The relative densities of the obtained cermets were obtained by two methods. One way was to calculate the relative densities based on the sintering linear shrinkage, according to the following Eq. (1) [19]:

$$\rho = \frac{\rho_1}{\rho_0(1-\Delta L/L_0)^3} \tag{1}$$

Where ρ is the relative density of sample, ρ_1 is the volume density of the green body (g cm^{-3}), ρ_0 is the theoretical density of the sample (g cm^{-3}), and $\Delta L/L_0$ is the linear shrinkage. Another way was to be measured by an Archimedes drainage method with deionized water as the immersion medium. The sample was firstly dried in a vacuum-drying oven and the dried sample mass (m_1) was weighed with the accuracy of 0.001 g. Then, the sample was immersed in distilled water in vacuum, so the pores in the sample could be filled with water. Finally, the sample was hung completely in distilled water on the hook of the balance, at the same time, m_2 was measured. The relative density (ρ) of the sample was calculated according to the following Eq. (2):

$$\rho = \frac{m_1 \times \rho_w}{m_2 \times \rho_0} \tag{2}$$

where ρ_w is the density of the distilled water.

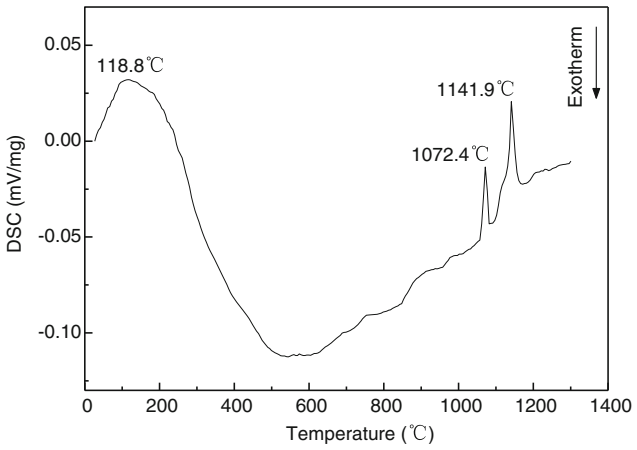

Fig. 1 DSC curve of $NiFe_2O_4$-based cermet adding with 15% metallic phase

The microstructure of fracture sections of samples was characterized by field emission scanning electron microscopy (Zeiss, Ultra Plus, Germany).

Results and discussion

Thermal analysis

Differential scanning calorimetry (DSC) was applied to analyze the phase evolution during the sintering process. The DSC curve of the $NiFe_2O_4$-based cermet adding with 15% metallic phase, heated at the rate of 10 °C/min in the nitrogen protective atmosphere, is shown in Fig. 1. It indicates that there are three endothermic peaks at 118.8 °C, 1072.4 °C, and 1141.9 °C, respectively. The broad endothermic peak around 118.8 °C is a result of the removal of free adsorbed water molecules. The melting points of Cu and 85Cu-15Ni binary alloy are respectively 1083.4 °C and 1158.6 °C according to the Cu-Ni binary alloy phase equilibrium diagram.

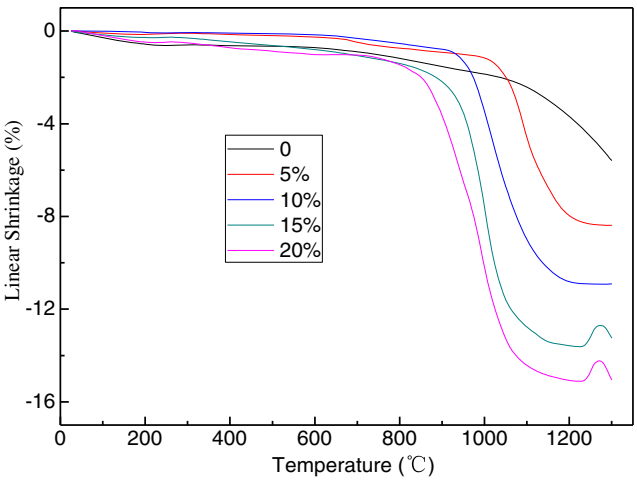

Fig. 2 Linear shrinkage versus temperature for samples with different metallic phase contents

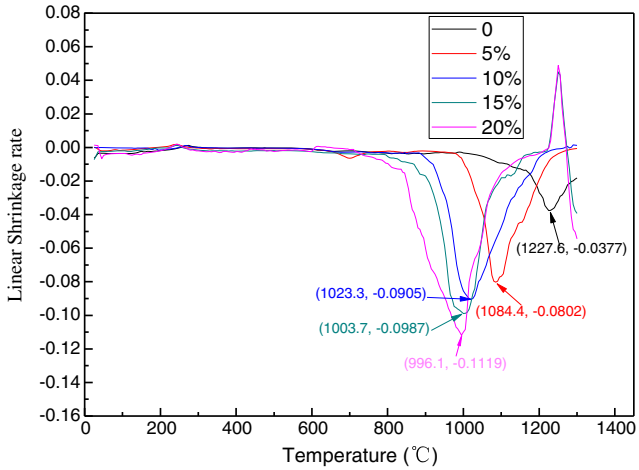

Fig. 3 Linear shrinkage rate versus temperature for samples with different metallic phase contents

When the temperature was over 1050 °C, major Cu powders firstly melt with the elevated temperature and then, the nickel atoms were dissolved solidly into the copper liquid phase. Finally, the 85Cu-15Ni binary alloy liquid phase was formed around 1141.9 °C. These results imply that the sintering temperature should be higher than 1141.9 °C to form a liquid phase sintering process, which could effectively promote sintering densification.

Sintering shrinkage behaviors

A constant heating rate of 10 °C/min was adopted to study the non-isothermal sintering behaviors of $NiFe_2O_4$-based green bodies. The linear shrinkage ($\Delta L/L_0$) of $NiFe_2O_4$-based green bodies with different metallic phase contents sintered at a constant heating rate of 10 °C/min is shown in Fig. 2. As shown in Fig. 2, the introduction of metallic phase is beneficial to enhancement of the maximum linear shrinkage from − 5.59 to − 15.11% with the metallic additive range from 0 to 20% ("−" meaning shrinkage). It can also be seen from Fig. 2 that the

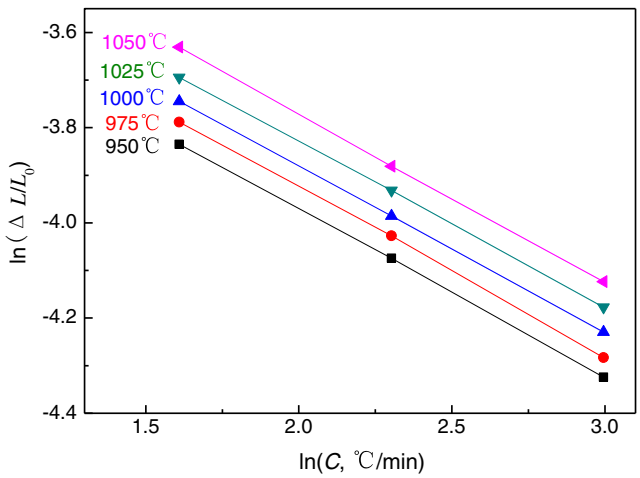

Fig. 4 $\ln(^{\Delta}L/L_0)_T$ versus ln$C$ for samples without the metallic phase

Table 1 The values of slope and linear regression coefficient (Y) of relationship between $\ln(\triangle L/L_0)_T$ and $\ln C$ for samples without the metallic phase under different temperatures

T/ °C	950	975	1000	1025	1050	Average
$-1/(m+1)$	−0.3527	−0.3570	−0.3494	−0.3482	−0.3553	−0.3525
Y	0.9956	0.9921	0.9902	0.9897	0.9924	

addition of the metallic phase shifts the onset of sintering towards lower temperatures from ~1066 for un-doped samples to ~837 °C for 20% metallic addition samples. When the temperature is over 1230 °C, the shrinkage is slightly reduced for the samples adding 15% and 20% metallic phase, maybe it is just because of the overflow of metallic phase.

Figure 3 shows the linear shrinkage rate ($d(\Delta L/L_0)/dt$) as a function of sintering temperature for $NiFe_2O_4$-based cermets with different metallic phase contents. It is obvious that the maximum linear shrinkage rate enhances with the increase of metallic phase content, while the temperature of maximum linear shrinkage rate (T_{max}) shows the opposite changing law. For example, when the metallic phase content increases from 5 to 20%, the maximum linear shrinkage rate improves from 0.0802 to 0.1119 and the T_{max} lowers from 1084.4 to 996.1 °C. These results suggest that the addition of the metallic phase can reduce the sintering temperature dramatically and promote the sintering densification process.

Sintering activation energy

The sintering process is traditionally classified into three stages, i.e., the initial, intermediate, and final stages of sintering [20]. Sintering activation energy of initial stage is a key parameter to understand the sintering mechanism. Sintering is a complex process and simulations for different stages of the sintering process are based on different sintering models. In this study, sintering activation energy of initial stage is calculated according to the linear shrinkage of initial stage. Bannister [21] suggested a general equation for isothermal initial-stage sintering as follows:

$$\frac{\mathrm{d}}{\mathrm{d}t}(\Delta L/L_0) = A_0 \exp\left(-\frac{Q}{RT}\right)/(\Delta L/L_0)^m \tag{3}$$

where $\Delta L/L_0$ is liner shrinkage, t is time, A_0 is a constant depending only on the material parameters and the sintering mechanisms, Q is sintering activation energy, R is molar gas constant, K is thermodynamic absolute temperature, and m is an exponent. The exponent, m, has values of $m = 0$ for viscous flow, $m = 1$ for volume diffusion, and $m = 2$ for grain boundary diffusion mechanisms. Under a constant heating rate condition, Culter [22] developed the Eq. (3) into the following equation:

$$(\Delta L/L_0)/T = A_1 \exp\left[-\frac{Q}{(m+1)RT}\right] \tag{4}$$

where A_1 is a constant. The natural logarithmic form of Eq. (4):

$$\ln[(\Delta L/L_0)/T] = -\frac{Q}{(m+1)R}\frac{1}{T} + \ln A_1 \tag{5}$$

If the exponent m can be determined, the sintering activation energy Q can be calculated from the slope a of plot $\ln[(\Delta L/L_0)/T]$ versus $1/T$ according to the formula of $Q = -(m+1)R \cdot a$.

According to the suggestion by Woolfrey et al. [23], the value m can be also determined by performing the experiments with different heating rates C, i.e., 5, 10, and 20 °C/min, according to the relationship between $\ln(\Delta L/L_0)_T$ and C, as follows:

$$\ln(\Delta L/L_0)_T = -\frac{\ln C}{m+1} + \ln A_2 \tag{6}$$

The computational derivation process of sintering activation energy of initial stage for sample without adding the metallic phase was taken as an example.

Firstly, the value m should be obtained on the basis of Eq. (6). The plots of $\ln(\triangle L/L_0)_T$ against $\ln C$ for the samples without adding the metallic phase are shown in Fig. 4. The linear fitting slopes and linear regression coefficient (Y) for different temperatures are listed in Table 1. It can be known that the

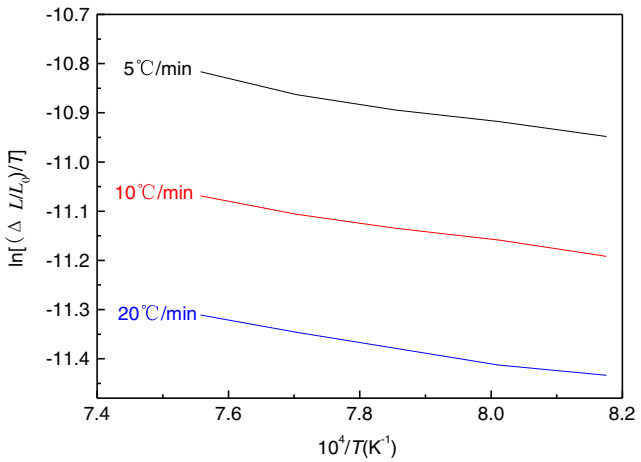

Fig. 5 $\ln[(\triangle L/L_0)/T]$ versus $1/T$ relation graph for sample without metallic phase

Table 2 The values of slope (a) and linear regression coefficient (Y) of relationship between $\ln[(\triangle L/L_0)/T]$ and $1/T$ for samples without metallic phase under different heating rates

Heating rate/ °C·min^{-1}	5	10	20	Average
a	− 20,556	− 19,269	− 20,099	− 19,975
Y	0.9719	0.9898	0.9854	

linear slope differs little and the linear regression coefficient is stable and close to 1, which indicates that the data has good repeatability and stability in the whole test process. The value of exponent m is calculated as 1.8369 according to the average slope.

Secondly, according to Eq. (5), the plots of $\ln[(\triangle L/L_0)/T]$ against $1/T$ for the samples without adding the metallic phase are shown in Fig. 5. The linear fitting slopes and linear regression coefficients (Y) at different temperatures are listed in Table 2. The linear shrinkages in nearly linear parts of curves at each heating rate were selected, which reflected only one dominant sintering mechanism during the initial stage of sintering [24]. The maximum absolute value of the fitted line slope is only 1.067 times that of the minimum value, implying the difference is not significant. It can be approximately considered that the three curves are parallel, indicating that the sample contraction change rate is close to each other under different heating rates. The average value of three slopes, − 19,975, is used to calculate the sintering activation energy Q as 471.13 kJ·mol^{-1} according to the formula of $Q = -(m+1)R \cdot a$, which is close to the value in our previous work [25].

According to the abovementioned calculation process, the exponent m and sintering activation energy Q of $NiFe_2O_4$-based cermets with different metallic phase contents are listed in Table 3. It can be seen from Table 3 that the exponent m decreases from 1.8369 to 1.0448 with the metallic additive range from 0 to 20%, while the sintering activation energy Q lowers from 471.13 to 236.47 kJ·mol^{-1}. It can be concluded that the initial stage sintering processes for samples with less than 20% metallic phase addition may be controlled by both grain boundary diffusion and volume-diffusion mechanisms, while only by volume-diffusion mechanism for sample with 20% metallic phase addition. In the initial stage sintering, the sintering temperature is lower than the melting point of copper or copper-nickel binary alloy so that there is no liquid phase generated. However, the atomic diffusion capacity of metallic phase is stronger than that of ceramic phase under the same condition. Therefore, the diffusion coefficient of the material is reinforced with the increase of metallic phase addition, resulting in the transformation from grain boundary diffusion to volume-diffusion and decrease of sintering activation energy. All of the above analysis results suggest that the introduction of the metallic phase could effectively promote the sintering process.

Microstructure

Based on Eq. (1), relative densities of the samples with various metallic phase contents as a function of sintering temperature (800–1300 °C) are sketched in Fig. 6. In addition, the green bodies with different metallic phase contents were sintered respectively to 1100 °C, 1150 °C, 1200 °C, 1250 °C, and 1300 °C at a constant heating rate of 10 °C/min, and then, the relative densities of these sintered samples were measured by the Archimedes drainage method and calculated according to Eq. (2), showing as chain lines in the same colors. It can be seen that the relative density calculated by sintering linear shrinkage is in good agreement with that measured by the Archimedes drainage method, except for samples adding 15% and 20% metallic phase when the temperature is over 1230 °C. It implies that there is a relatively big error for the relative density calculated by sintering linear shrinkage, owing to the overflow of the metallic phase. What's more, for the $NiFe_2O_4$-based cermets, the relative density increases slowly when the temperature exceeds 1200 °C.

The microstructures and relative densities of samples with different metallic phase contents sintered in a nitrogen shield atmosphere at 1200 °C for 6 h are shown in Figs. 7 and 8 respectively. It can be seen from Fig. 7 that the grains grow gradually and grain boundary cohesion becomes stronger as the increase of metallic phase content. Without adding the metallic phase, the $NiFe_2O_4$-based ceramic grains just like heaping with lots of pores, as a result, the relative density is

Table 3 Values of exponent m and sintering activation energy Q for samples with different metallic phase contents at the initial stage of sintering

Metallic phase content/%	0	5	10	15	20
m	1.8369	1.5687	1.3747	1.1873	1.0448
Q/kJ·mol^{-1}	471.13	376.87	322.35	270.14	236.47

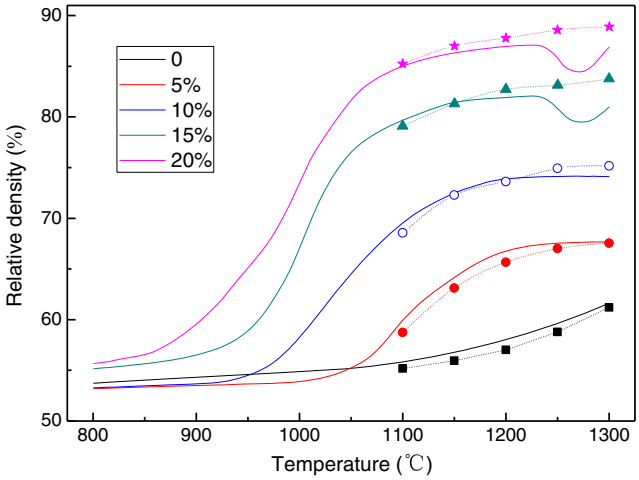

Fig. 6 Relative densities of the samples with various metallic phases as a function of temperature

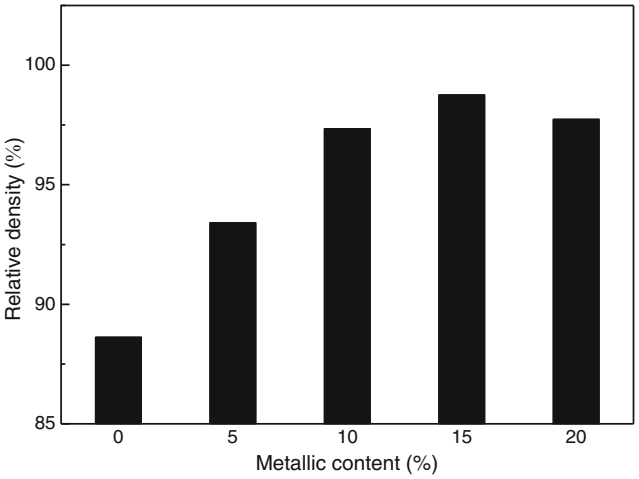

Fig. 8 Relative densities of samples with different metallic phase contents sintered in a nitrogen shield atmosphere at 1200 °C for 6 h

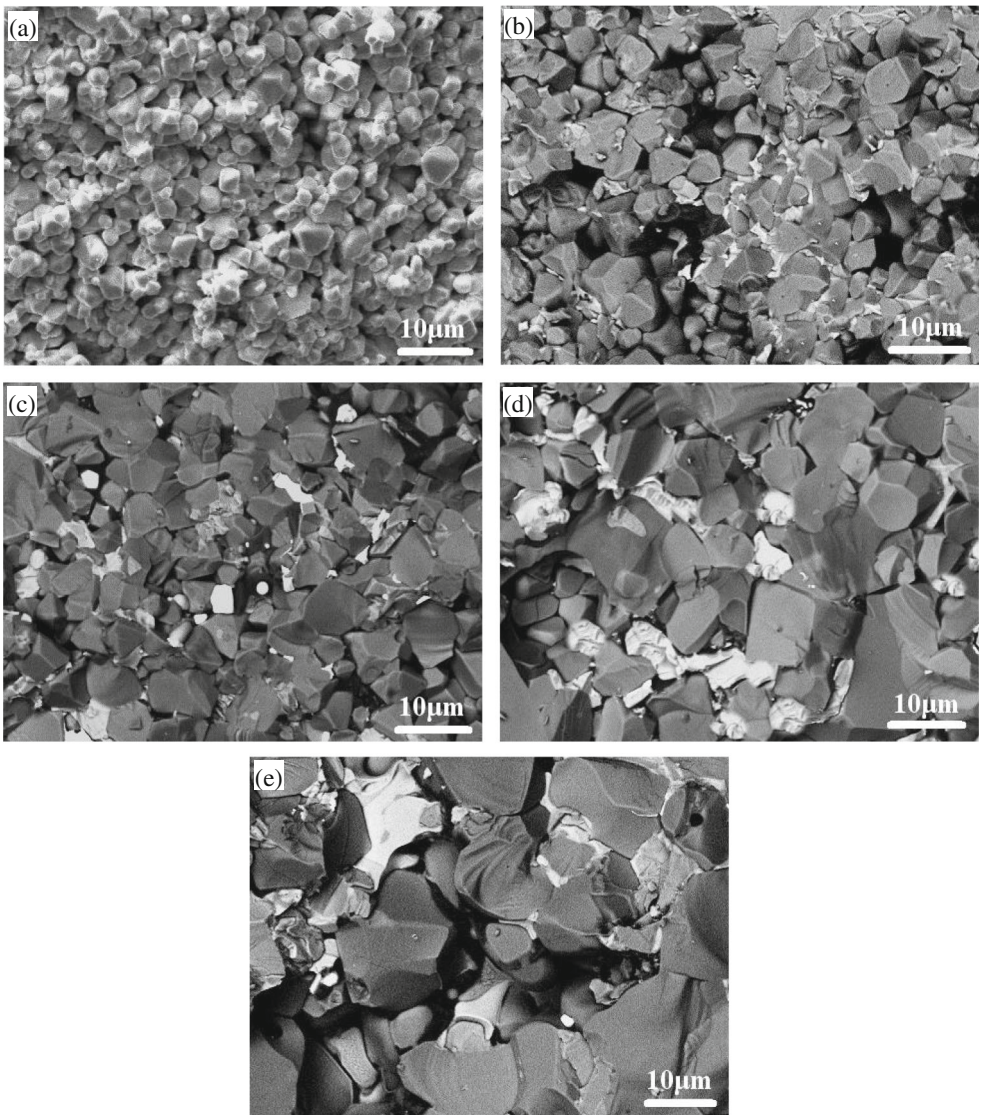

Fig. 7 SEM photographs of samples with different metallic phase contents sintered in a nitrogen shield atmosphere at 1200 °C for 6 h. **a** 0%. **b** 5%. **c** 10%. **d** 15%. **e** 20%

as low as 88.62%. The average grain size is relatively small and the gap between grains is large, resulting in the weak grain boundary cohesion. It signifies that the sintering temperature should be higher than 1300 °C for dense $NiFe_2O_4$-based ceramics. There is a major change of microstructure for the $NiFe_2O_4$-based cermets with the introduction of the metallic phase. As the increase of the metallic phase content from 5 to 15%, the sintered $NiFe_2O_4$-based cermets become denser and the relative density increases from 93.41 to 98.76%. Meanwhile, the grains of the sintered cermets grow up step-by-step and the grain boundary bonding strength becomes stronger and transgranular fracture becomes dominant. In this research, the sintering temperature (1200 °C) is somewhat higher than the melt point of the 85Cu-15Ni alloy (1175 °C); therefore, the cermets undergo the liquid sintering process. The existing metallic phase in the sintering process can be filled in the blanks between the NiO-$NiFe_2O_4$ ceramic grains by capillarity. So the porosity decreases with the increase of metallic content. When the metallic phase content is 20%, the relative density reduces slightly for some metallic microspheres on the surface of sintered $NiFe_2O_4$-based cermet. Some micropores among ceramic grains are formed, originating from the overflow of the metallic phase. It suggests that the sintering temperature should be a bit lower for $NiFe_2O_4$-based cermet with more than 20% metallic phase content. A proper metallic phase content should be selected between 15 and 20% to obtain highly dense $NiFe_2O_4$-based cermets.

Conclusions

$NiFe_2O_4$-based cermet inert anodes adding different metallic phase contents have been synthesized with the purpose of replacing carbon anodes in aluminum electrolysis. The sintering behavior shows that the linear shrinkage and linear shrinkage rate enhances with the increase of metallic phase contents, while the temperature of maximum linear shrinkage rate displays the opposite changing law. The addition of the metallic phase shifts the onset of sintering towards lower temperatures from ~1066 for un-doped samples to ~837 °C for 20% metallic addition samples. As the content of metallic phase increases from 0 to 20%, the sintering activation energy of the initial stage lowers from 471.13 to 236.47 $kJ \cdot mol^{-1}$. The grains grow gradually and grain boundary cohesion becomes stronger as the increase of metallic phase content. When the metallic phase content ranges from 5 to 15%, the $NiFe_2O_4$-based cermets sintered at 1200 °C for 6 h become denser and the relative density increases from 93.41 to 98.76%. The results suggest that the introduction of metallic phase could effectively promote the sintering process.

Funding information The authors gratefully acknowledge the financial support from the Fundamental Research Funds for the Central Universities (N182504015).

References

1. Kvande, H., Haupin, W.: Inert anodes for Al smelters: energy balances and environmental impact. JOM. **53**(5), 29–33 (2001)
2. Sadoway, D.R.: Inert anodes for the Hall-Héroult cell: the ultimate materials challenge. JOM. **53**(5), 34–35 (2001)
3. Keniry, J.: The economics of inert anodes and wettable cathodes for aluminum reduction cells. JOM. **53**(5), 43–37 (2001)
4. Feng, L.C., Shao, W.Z., Zhen, L., Xie, N., Ivanov, V.V.: Cu_2O/Cu cermet as a candidate inert anode for Al production. Int J Appl Ceram Technol. **4**(5), 453–462 (2007)
5. Olsen, E., Thonstad, J.: Nickel ferrite as inert anodes in aluminum electrolysis: part I material fabrication and preliminary testing. J Appl Electrochem. **29**(3), 293–299 (1999)
6. Xi, J.H., Xie, Y.J., Yao, G.C., Liu, Y.H.: Effect of additive on corrosion resistance of $NiFe_2O_4$ ceramics as inert anodes. Trans Nonferrous Metals Soc. China. **18**(2), 356–360 (2008)
7. Du, J.J., Liu, Y.H., Yao, G.C., Long, X.L., Zu, G.Y., Ma, J.: Influence of MnO_2 on the sintering behavior and magnetic properties of $NiFe_2O_4$ ferrite ceramics. J Alloys Compd. **510**(1), 87–91 (2012)
8. Liu, B.G., Zhang, L., Zhou, K.C., Li, Z.Y., Wang, H.: Electrical conductivity and molten salt corrosion behavior of spinel nickel ferrite. Solid State Sci. **13**(8), 1483–1487 (2011)
9. Nightingale, S.A., Longbottom, R.J., Monaghan, B.J.: Corrosion of nickel ferrite refractory by Na_3AlF_6-AlF_3-CaF_2-Al_2O_3 bath. J Eur Ceram Soc. **33**(13–14), 2761–2765 (2013)
10. Lai, Y.Q., Tian, Z.L., Li, J., Ye, S.L., Li, X.Z., Liu, Y.X.: Results from 100 h electrolysis testing of $NiFe_2O_4$ based cermet as inert anode in aluminum reduction. Trans Nonferrous Metals Soc. China. **16**(4), 970–974 (2006)
11. Ma, J., Bao, L., Yao, G.C., Liu, Y.H., Zhang, X., Zhang, Z.G., Liang, L.S.: Effect of MnO_2 addition on properties of $NiFe_2O_4$-based cermets. Ceram Int. **37**(8), 3381–3387 (2011)
12. Tian, Z.L., Lai, Y.Q., Li, J., Liu, Y.X.: Electrical conductivity of Cu/(10NiO-$NiFe_2O_4$) cermet inert anode for aluminum electrolysis. J Cent S Univ Technol. **14**(5), 643–646 (2007)
13. Tian, Z.L., Lai, Y.Q., Li, J., Liu, Y.X.: Effect of Ni content on corrosion behavior of Ni/(10NiO-90$NiFe_2O_4$) cermet inert anode. Trans Nonferrous Metals Soc China. **18**(2), 361–365 (2008)
14. Tian, Z.L., Guo, W.C., Lai, Y.Q., Zhang, K., Li, J.: Effect of sintering atmosphere on corrosion resistance of Ni/($NiFe_2O_4$–10NiO) cermet inert anode for aluminum electrolysis. Trans Nonferrous Metals Soc China. **26**(11), 2925–2929 (2016)
15. Xi, J.H., Liu, Y.H., Yao, G.C.: Effects of technological conditions on properties of inert anodes of Ag/$NiFe_2O_4$ cermet. Mater Sci Technol. **16**(1), 41–43 (2008) 48 (in Chinese)
16. Li, W.X., Zhang, G., Li, J., Lai, Y.Q.: $NiFe_2O_4$-based cermet inert anodes for aluminum electrolysis. JOM. **61**(5), 39–43 (2009)
17. Zhang, G., Li, J., Lai, Y.Q., Tian, Z.L.: Effect of metallic phase content on mechanical properties of (85Cu-15Ni)/(10NiO-$NiFe_2O_4$) cermet inert anode for aluminum electrolysis. Trans Nonferrous Metals Soc China. **17**(5), 1063–1068 (2007)
18. Du, J.J., Yao, G.C., Liu, Y.H., Ma, J., Zu, G.Y.: Influence of V_2O_5 as an effective dopant on the sintering behavior and magnetic properties of $NiFe_2O_4$ ferrite ceramics. Ceram Int. **38**(2), 1707–1711 (2012)
19. Mitra, S., Kulkarni, A.R., Prakash, O.: Densification behaviour and two stage master sintering curve in lithium sodium niobate ceramics. Ceram Int. **39**(S1), S65–S68 (2013)

20. Coble, R.L.: Sintering crystalline solids. I. Intermediate and final state diffusion models. J Appl Phys. **32**(5), 787–792 (1961)
21. Bannister, M.J.: Shape sensitivity of initial sintering equations. J Am Ceram Soc. **51**(10), 548–553 (1968)
22. Keski, J.R., Cutler, I.B.: Initial sintering of MnXO-Al_2O_3. J Am Ceram Soc. **51**(8), 440–444 (1968)
23. Woolfrey, J.L., Bannister, M.J.: Nonisothermal techniques for studying initial-stage sintering. J Am Ceram Soc. **55**(8), 390–394 (1972)
24. Zhang, T.S., Peter, H., Huang, H.T., Kilner, J.: Early-stage sintering mechanisms of Fe-doped CeO_2. J Mater Sci. **37**(5), 997–1003 (2002)
25. Zhang, Z.G., Yao, G.C., Luo, H.J., Zhang, X., Ma, J.F., Xu, J.R.: Sintering behavior and properties of $NiFe_2O_4$ ceramic inert anode toughened by adding $NiFe_2O_4$ nanopowder. J Inorg Mater. **31**(7), 761–768 (2016)